Bull. Mater. Sci., Vol. 36, No. 3, June 2013, pp. 417–427. © Indian Academy of Sciences.

Synthesis, non-isothermal crystallization and magnetic properties of $Co_{0.75}Zn_{0.25}Fe_2O_4$/poly(ethylene-co-vinyl alcohol) nanocomposite

TAIEB AOUAK*, NASRALLAH M DERAZ and ABDULLAH S ALARIFI
Chemistry Department, College of Science, King Saud University, P.O. Box 2455, Riyadh 11451, Saudi Arabia

MS received 11 March 2012; revised 26 May 2012

Abstract. **The synthesis of $Co_{0.75}Zn_{0.25}Fe_2O_4$/poly(vinyl alcohol-co-ethylene) (ferrite/PEVA) nanocomposite was carried out through two steps: impregnation of the ferrite particules by PEVA and then mixing the ferrite/PEVA impregnated with PEVA solution. A non-isothermal study of the crystallization kinetic of ferrite/PEVA nanocomposite was carried out by differential scanning calorimetry (DSC), scanning electron microscope (SEM) and X-ray diffraction (XRD) techniques. It was observed that the Ozawa equation describes perfectly the primary process of non-isothermal crystallization of ferrite/PEVA system. There is a strong dependence of the ferrite/PEVA composition on the crystallization parameters. The crystallization activation energy (E_a) calculated from the Xu and Uhlmann model increased by increasing the ferrite content in ferrite/PEVA nanocomposites between 3 and 7 wt% and decreased dramatically beyond these values. The results revealed that the ferrite nanoparticles were uniformly distributed throughout the PEVA matrix. The percentage of magnetization of the composite decreases as the concentration of the ferrite increases.**

Keywords. **$Co_{0.75}Zn_{0.25}Fe_2O_4$; poly(vinyl alcohol-co-ethylene); nanocomposite; non-isothermal crystallization, magnetization.**

1. Introduction

Polymer-based composites have attracted the attention of researchers due to their flexibility, tunable properties and easy processibility. The composites based on ferrite–polymer mixtures have been of much interest, owing to their dielectric and magnetic properties. Co–ferrite (Vaishnava *et al* 2006), NiZn–ferrite (Nakamura *et al* 1994) and MnZn–ferrite (Yavuz *et al* 2005; Kazantseva *et al* 2006), as exemplary composites, have potential applications in various areas such as information storage media (ISM), electromagnetic interference shielding (EIS) (Pant *et al* 1995; Matsumoto and Miyata 2002; Slama *et al* 2003), drug delivery (Gomez-Lopera *et al* 2001), drug targeting and contrasting agents in magnetic resonance imaging (MRI) (Arshady 1993; Wiltshire *et al* 2001). The impregnation of magnetic fillers in the polymer matrix imparts the magnetic properties and modifies the physical properties of the matrix considerably. However, mechanical properties of the polymer bonded magnets depend strongly on the properties of polymer matrix, magnetic fillers and interfacial condition between the investigated components (Xiao and Otaigbe 2000). Further, the surface area of the filler and the volume fraction of nanoparticles are a primary factor in controlling the mean distance between particles.

On the other hand, poly(vinyl alcohol-co-ethylene) (PEVA) membranes have attracted research interest in fields of biomedical science and water treatment because of their good blood compatibility and hydrophilicity (Young *et al* 1997; Montoya *et al* 2006). PEVA has been widely used as food packing material due to its excellent gas barrier properties and harmlessness to health. PEVA, in their different compositions, are essentially randomic and semicrystalline, over the entire range of composition, despite the irregularity and non-steriospecificity of the vinyl alcohol units distributed on the PEVA copolymer chain (Keskin and Elliot 2003). No doubt that blending PEVA with ferrite would increase its utilization in different domains cited above. Several investigations were reported on morphology and crystallinity behaviour of this copolymer or that blended with other polymers, but no investigations were reported on the study of PEVA/ferrite nanocomposites.

To achieve such a goal we have chosen the $Co_{0.75}Zn_{0.25}Fe_2O_4$ as ferrite nanoparticles with magnetization of 58 emu/g and 30–70 nm particle size. In the present study, an attempt has been made to identify the effect of ferrite ratios on the structure, morphology and non-isothermal properties of the $Co_{0.75}Zn_{0.25}Fe_2O_4$/PEVA system. The magnetic properties of these composites were also studied. The employed techniques were DSC, SEM, XRD and VSM.

2. Experimental

2.1 *Materials*

Poly(ethylene-co-vinyl alcohol) (PEVA) molecular weight = 29,000, containing 38 mole% of ethylene unit

*Author for correspondence (taouak@yahoo.fr)

was purchased from Aldrich, Germany. The average number of molecular weight of this polymer was 29,000. Dimethyl formamide (DMF) was purchased from Aldrich. $Co(NO_3)_2{\cdot}6H_2O$, $Zn(NO_3)_2{\cdot}6H_2O$, $Fe(NO_3)_3{\cdot}9H_2O$ and urea were purchased from (BDH, UK). All materials were used as received.

2.2 *Preparation of $Co_{0.75}Zn_{0.25}Fe_2O_4$ nanoparticles*

$Co_{0.75}Zn_{0.25}Fe_2O_4$ (cobalt–zinc ferrite) powder having a coercive force of 500 kOe, magnetization, 58 emu/g and 30–70 nm particle size were prepared by a combustion route. Detailed procedure was reported elsewhere (Deraz *et al* 2009). This sample was prepared by mixing calculated proportions of cobalt, zinc and iron nitrates with a certain amount of urea. The formula of ferrite was determined by XRD analysis.

2.3 *Preparation of $Co_{0.75}Zn_{0.25}Fe_2O_4$/PEVA nanocomposites*

Ferrite/PEVA nanocomposites were prepared in two steps: (a) Impregnation of $Co_{0.75}Zn_{0.25}Fe_2O_4$ nanoparicles: 0·2 g of PEVA was dissolved in 20 mL of DMF at 80 °C and the solution was placed into a 250 mL round-bottom flask. After the addition of a known amount of ferrite, the slurry was well swirled before evaporating the solvent to dryness through a rotary evaporator. The impregnated ferrite powder was further dried in a vacuum at 60 °C for 48 h. (b) The dried solid powder was then sieved before mixing with a concentrated PEVA solution at 60 °C for 10 min. It was noted that at this temperature and time duration, the dried PEVA swells in DMF while the PEVA dissolved at 80 °C remains in solution as shown in scheme 1. The films of $Co_{0.75}Zn_{0.25}Fe_2O_4$/PEVA nanocomposites were prepared by solution casting from DMF by slow evaporation at 60 °C for 1 week; the residual solvent was removed under vacuum at 80 °C for about 3 days. The preparation conditions of $Co_{0.75}Zn_{0.25}Fe_2O_4$/PEVA nanocomposites are gathered in table 1.

2.4 *Differential scanning calorimeter (DSC)*

The glass transition temperature (T_g), melting point (T_m), crystallization temperature (T_p) and heat of crystallization (ΔH_c) of PEVA and composites were measured with a DSC (Setaram Labsys DSC 16). Samples weighing between 10 and 12 mg were packed in aluminum DSC pans before placing in DSC cell. The samples were heated from 30 to 240 °C at a heating rate of 20 °C min^{-1} and kept at 200 °C for 10 min in order to destroy all nuclei that might act as seed crystals. The samples were then cooled down to 30 °C at constant rates of 5, 10, 20 and 30 °C/min^{-1}, respectively. The data were collected from the second scan. No degradation phenomenon of PEVA and $Co_{0.75}Zn_{0.25}Fe_2O_4$/PEVA nanocomposites were observed in all the thermograms. This finding was also confirmed by solubility test realized after DSC analysis. The glass transition temperature was taken as the midpoint in the heat capacity change with temperature. On the other hand, the melting and crystallization points were taken at the summits of the peaks.

Table 1. Preparation conditions of $Co_{0.75}Zn_{0.25}Fe_2O_4$/PEVA nanocomposites.

Notation	Ferrite/PEVA system composition (wt%)	PEVA (g)	Ferrite (g)	DMF (mL)
C_1	2:98	0·20	0·0041	20
C_2	5:95	0·20	0·011	20
C_3	7:93	0·20	0·015	20
C_4	10:90	0·20	0·022	20

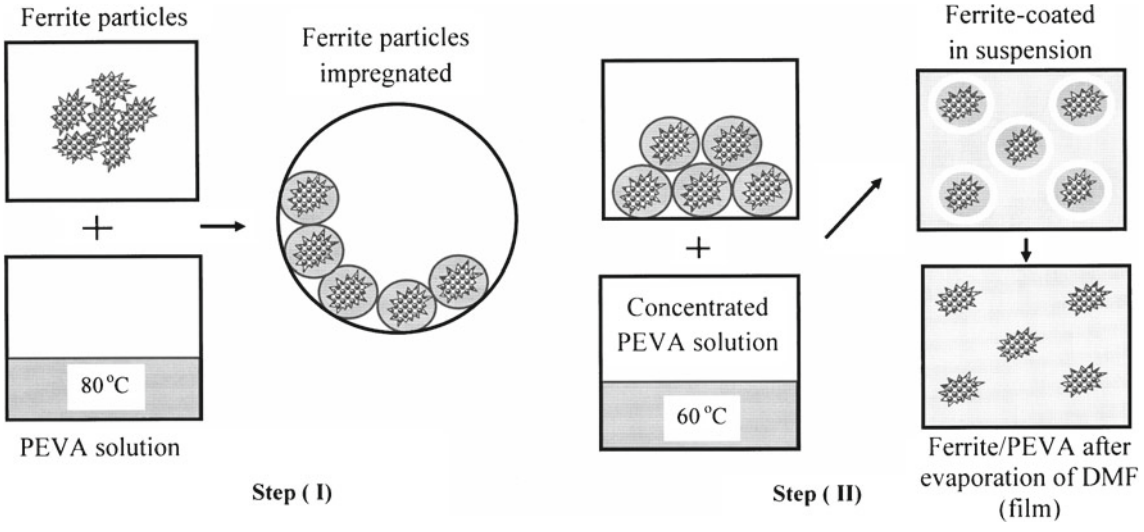

Scheme 1. Preparation steps of $Co_{0.75}Zn_{0.25}Fe_2O_4$/PEVA nanocomposites.

2.5 *Scanning electron microscope (SEM)*

Scanning electron micrographs (SEMs) of ferrite, polymer and composites were recorded on JEOL JSM-6380 LA electron microanalysis. The specimens were dispersed over gold grids.

2.6 *Vibrating sample magnetometer (VSM)*

The magnetic properties of the ferrite sample were measured at room temperature using a vibrating sample magnetometer (VSM; 9600-1 LDJ, USA) in a maximum applied field of 15 kOe. The saturation magnetization (M_s), remanence magnetization (M_r) and coercivity (H_c) were estimated from the obtained hysteresis loops.

2.7 *XRD analysis*

X-ray measurement of bulk $Co_{0.75}Zn_{0.25}Fe_2O_4$, pure PEVA and $Co_{0.75}Zn_{0.25}Fe_2O_4$/PEVA nanocomposites with different ferrite contents was carried out using a BRUKER D8 advance diffractometer (Germany). The patterns were run with CuKα radiation at 40 kV and 40 mA with scanning speed in 2θ of 2° min^{-1}.

3. Calculations

The crystallite size of $Co_{0.75}Zn_{0.25}Fe_2O_4$ nanoparticles was calculated by using Scherrer equation (Cullity 1976) having X-ray diffraction line broadening:

$$d = \frac{B\lambda}{\beta \cos\theta}, \tag{1}$$

where d is the average crystallite size of the phase under investigation, B the Scherrer constant (0·89), λ the wavelength of X-ray beam used, β the full width at half maximum (FWHM) of diffraction and θ the Bragg's angle.

The degree of crystallinity (X_c) was obtained from the enthalpy evolved during crystallization using the following relationship (Hammami *et al* 1995):

$$X_c\,(\%) = \frac{\Delta H_c}{(1-\varphi)\times \Delta H_m} \times 100, \tag{2}$$

where ΔH_c is the apparent enthalpy of crystallization, ΔH_m the extrapolated enthalpy corresponding to the melting of a 100% crystalline sample with an average value of 68·62 Jg^{-1} (Young *et al* 1997) and φ the weight fraction of $Co_{0.75}Zn_{0.25}Fe_2O_4$ in the composite.

The relative degree of crystallinity, X_T, as a function of crystallization temperature was obtained from the following equation (Jeziorny 1978):

$$X_T = \frac{\int_{T_0}^{T}\left(\frac{dH}{dt}\right)dt}{\int_{T_0}^{T\infty}\left(\frac{dH}{dt}\right)dt}, \tag{3}$$

where T_0 and T_∞ are the starting and finishing crystallization temperatures taken at the starting and finishing inflections of the crystallization peak, respectively and H the enthalpy of the process. After substituting areas of DSC curves, (3) becomes

$$X_T = \frac{A_T}{A_\infty}, \tag{4}$$

where A_T is the area under the DSC curves from $T = T_0$ to $T = T$ and A_∞ the total area under the crystallization curve. Based on (4), X_T at a specific temperature was calculated. During non-isothermal crystallization, variation of crystallization time with crystallization temperature obeyed the following equation:

$$t = \frac{T_0 - T}{\beta}, \tag{5}$$

where T is the temperature at crystallization time, t and β the cooling rate.

Although many models have been developed for isothermal crystallization kinetics, only the models from Jeziorny (1978), Ziabicki (1996) and Ozawa (1971) are suitable for non-isothermal kinetics. In the present study, the Ozawa relationship:

$$1 - X_T = \exp\left(-\frac{k_T}{\beta^m}\right), \tag{6}$$

was adopted to investigate the non-isothermal crystallization of the pure polymer and the blend at various cooling rates and was extended from the Avrami (1937) equation:

$$1 - X_t = \exp\left(-kt^n\right), \tag{7}$$

originally applied for isothermal crystallization to non-isothermal crystallization by assuming that the sample is cooled at a constant cooling rate. Here X_t and X_T are the relative degrees of crystallinity as a function of crystallization time and temperature, respectively, k the crystallization kinetics rate constant, k_T the cooling function of non-isothermal crystallization at temperature T, t the crystallization time, β the cooling rate, n the isothermal Avrami exponent and m the Ozawa exponent depending on the dimension of crystal growth. The m or n close to 3 indicates bulk or three-dimensional crystal growth and m or n close to 1 indicates surface growth. Intermediate values of n between 1 and 3 indicate that surface and internal crystallizations occur simultaneously (Francis 2005). Equation (6) can be linearized as follows:

$$\ln\left(-\ln\left(1 - X_T\right)\right) = \ln k_T - m\,\ln\beta. \tag{8}$$

The Ozawa equation can be used to analyse the non-isothermal crystallization process.

The crystallization activation energy (E_a) can be calculated using Kissinger equation (Kissinger 1956)

$$E_a = \frac{d\left(\ln\left(\beta/T_p^2\right)\right)}{d\left(1/T_p\right)}R, \tag{9}$$

where R is an universal gas constant, T_p the crystallization temperature (in Kelvin) taken at the summits of the crystallization peaks.

After plotting $\ln\left(\beta/T_p^2\right)$ vs $1/T_p$, the crystallization activation energy (E_a) can be obtained. Xu *et al* (1991) and Yinnon and Uhlman (1983) proposed that the Kissinger model is only valid when crystal growth occurs on a specified number of nuclei. They modified the Kissinger equation to account for nucleation and crystallization growth occurring simultaneously to

$$E_a = \frac{d\left[\ln\left(\beta^{n/m}/T_p^2\right) \times R\right]}{m \times d\left(1/T_p\right)}, \tag{10}$$

where m represents the dimensionality of the crystalline phase. The n and m are correlated to each other through the relation $m = n-1$.

4. Results and discussion

4.1 *Morphology and microstructure*

SEM photographs were used to evaluate the surface morphology and size distribution of the as-prepared samples. Figure 1(a–c) shows SEM images of the $Co_{0.75}Zn_{0.25}Fe_2O_4$, PEVA and their composite at 10 wt% of ferrite taken as example, respectively. This figure reveals remarkable changes in the microstructure, regarding grain size and particle distribution of the as-prepared system by mixing the polymer with a certain amount of the ferrite studied. In the ferrite sample (figure 1a), one can see the formation of multigrain agglomerations which consist of very fine crystallites with spongy structure due to the release of a large amount of gases during combustion process. The size of the particle varies from 30 to 70 nm, which is in good agreement with the crystallite size determined by XRD analysis. It has been seen in figure 1(b) that the polymer is homogeneously shaped.

During metallographic observation of powders' morphology and fracture's surfaces of the composite's samples, it was observed that the distribution of powders of Co–Zn ferrite in polymer matrix has been irregular. These powder particles have spherical shape in the polymer matrix (figure 1c). The fact that the magnetic particles as filler are nanosize, randomly oriented, uniformly dispersed and isolated from each other as seen in figure 1(c). These findings resulted in reduction of the particles' surface energy, which controls the mean distance between particles during a mixing process which reduces the agglomeration inside the ferrite–polymer samples especially at a relatively high loading level. This indicates that the dispersion and homogeneity of the ferrite powders are improved with the presence of the polymer materials. In other words, the ferrite multigrain agglomerations were perfectly coated and distributed homogeneously in the PEVA matrix as planned in scheme 1. However, incorporation of the ferrite powders in the matrix of the investigated polymer may lead to a modification in the different properties of the polymer studied as well as formation of a new polymer-bonded magnet.

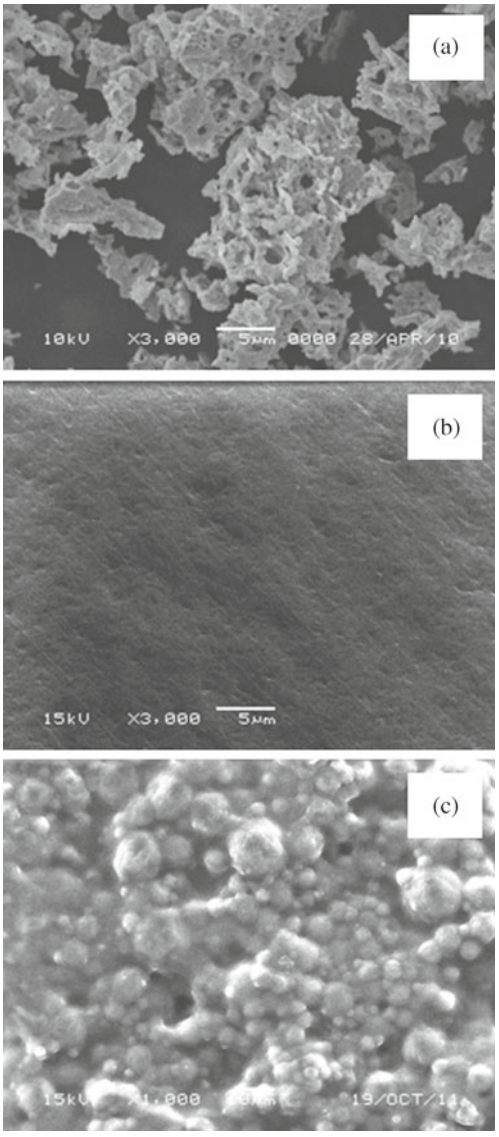

Figure 1. SEM images of: (**a**) bulk $Co_{0.75}Zn_{0.25}Fe_2O_4$; (**b**) pure PEVA and (**c**) $Co_{0.75}Zn_{0.25}Fe_2O_4$/PEVA system with 10 wt% of ferrite content (C_4).

4.2 *Structural analysis*

XRD patterns of $Co_{0.75}Zn_{0.25}Fe_2O_4$, PEVA and their composites at 5 and 10 wt% of ferrite content are shown in figure 2. Inspection of this figure revealed that: (i) The PEVA specimen consisted of well-crystalline polymer particles. (ii) The observed diffraction peaks for ferrite sample are perfectly indexed to zinc-substituted cobalt ferrite, $Co_{0.75}Zn_{0.25}Fe_2O_4$ phase (JCPDS card no. 22-1086) with different planes (2 2 0), (3 1 1), (4 0 0), (5 1 1) and (4 4 0) of cubic spinel structure. (iii) The ferrite–polymer samples

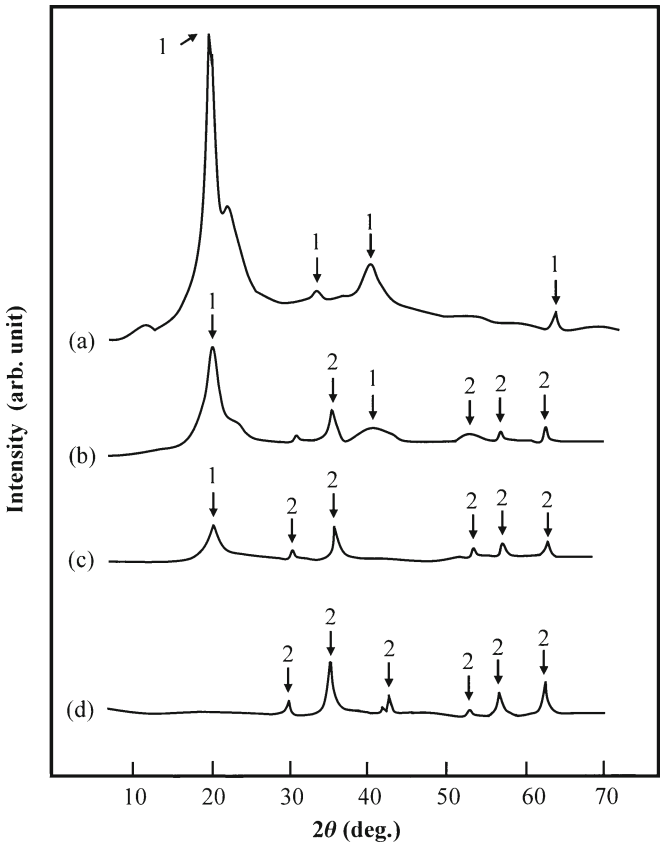

Figure 2. XRD patterns of: (**a**) pure PEVA; (**b**) $Co_{0.75}Zn_{0.25}Fe_2O_4$/PEVA (5:95 wt%)($C_2$); (**c**) $Co_{0.75}Zn_{0.25}Fe_2O_4$/PEVA (10:90 wt%) ($C_4$) and (**d**) bulk $Co_{0.75}Zn_{0.25}Fe_2O_4$ nanoparticles: line (1) PEVA and line (2) $Co_{0.75}Zn_{0.25}Fe_2O_4$.

consisted of all the diffraction lines corresponding to polymer and $Co_{0.75}Zn_{0.25}Fe_2O_4$ crystallites. The incorporation of the ferrite powder in the polymer matrix led to a decrease in the degree of crystallinity of the polymer particles depending upon the decrease in the peak height related to this polymer. The augmentation of the ferrite concentration enhanced the decrease in crystallinity of the polymer particles. In other words, the highly filled ferrites might hinder the motion of polymer segments with a subsequent increase in the ferrite dispersion of highly filled particles in polymer matrix (Guschl *et al* 2002). This conclusion might find evidence from small shift of the diffraction peaks of ferrite and polymer to higher Bragg's angle with an increase in the concentration of ferrite added. Indeed, the main diffraction lines of polymer and ferrite shifted from $2\theta = 20°$ and 35·074° to $2\theta = 20{\cdot}095°$ and 35·101°, respectively. (iv) The presence of the ferrite powders in the polymer matrix brought about a decrease in the peaks height of the Co–Zn ferrite crystallites indicating to the decrease in the crystallite size of these crystallites. The increase in the ferrite concentration led to slight increase in the crystallite size of the ferrite due to weak agglomeration process between the ferrite particles inside the polymer matrix. The crystallite size of the synthesized zinc-substituted cobalt ferrite samples estimated from X-ray peak broadening of the (3 1 1) peak using Scherrer formula (Cullity 1976). The crystallite size of the investigated ferrite decreases from 70 to 30 nm by increasing the amount of this ferrite inside the polymer matrix. This indicates that the incorporation of ferrite in the polymer matrix brought about reduction of the agglomeration of the ferrite nanoparticles leading to lowering the crystallite size of ferrite.

4.3 *Thermal behaviour of $Co_{0.75}Zn_{0.25}Fe_2O_4$/PEVA nanocomposite*

For uniform thermal history in all samples, the thermograms represented the results of a second run after quenching from temperatures just above the T_g. All thermograms clearly showed that there is only one T_g and one T_m for the PEVA and each composite, and also the dependence of T_g and T_m on the molar ratio of the ferrite added. The T_g and T_m values of the PEVA and the composites are given in table 2. As seen in table 2, the T_g of the composites increased as the $Co_{0.75}Zn_{0.25}Fe_2O_4$ content increased. In other words, the maximum increase in the T_g and T_m values of the investigated polymer was due to the treatment with 5 wt% of $Co_{0.75}Zn_{0.25}Fe_2O_4$ attaining 23·6 and 5·4%, respectively. This phenomenon was also observed by different authors using other polymeric systems (Utracki *et al* 1989; Kuo *et al* 2005; Li *et al* 2005; Lin *et al* 2006) and may be explicable in terms of thermodynamic mixing accompanied by exothermic interaction between a crystalline polymer and the particles.

DSC cooling thermograms of PEVA and $Co_{0.75}Zn_{0.25}Fe_2O_4$/PEVA system containing 2 (C_1), 5 (C_2) and 10 (C_4) wt% of $Co_{0.75}Zn_{0.25}Fe_2O_4$ content at different cooling rates are shown in figure 3. The thermograms of the pure PEVA and all the composites were similar to each other, and there was only one obvious crystallization peak (T_p) between 130 and 147 °C, showing an analogue crystallization behaviour of the pure PEVA and $Co_{0.75}Zn_{0.25}Fe_2O_4$/PEVA systems. In both cases, T_p shifted to the lower temperature as the cooling rate increased. The

Table 2. DSC data for PEVA and $Co_{0.75}Zn_{0.25}Fe_2O_4$/PEVA nanocomposites.

System $CoZnFe_2O_4$/PEVA (g:g)	T_g (°C)	T_m (°C)	E_a (KJ mol $^{-1}$)
0:100	55	167	233
2:98	56	168	237
5:95	63	176	381
7:93	65	173	449
10:90	67	172	417

T_g and T_m have been determined with 20 °C/min cooling rate.

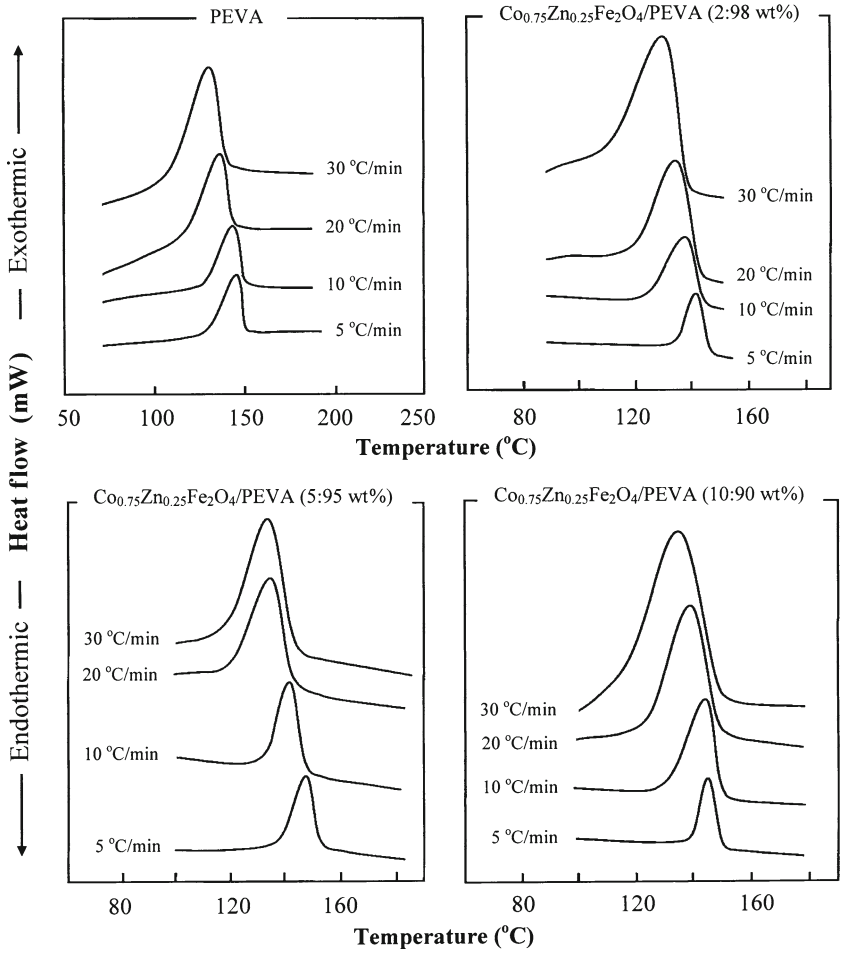

Figure 3. DSC thermograms at different cooling rates of pure PEVA and $Co_{0.75}Zn_{0.25}Fe_2O_4$/PEVA nanocomposites in wt%.

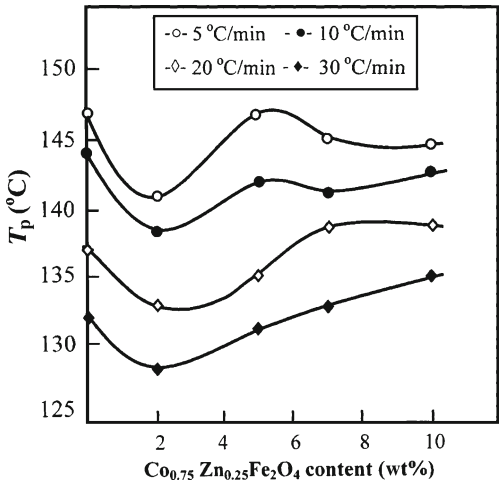

Figure 4. Relation between T_p (K) and composition of $Co_{0.75}Zn_{0.25}Fe_2O_4$/PEVA in wt%.

influence of incorporating of $Co_{0.75}Zn_{0.25}Fe_2O_4$ on the non-isothermal crystallization kinetics of PEVA was considered. As shown in figure 4, T_p passed by a minimum value in the presence of 2 wt% of $Co_{0.75}Zn_{0.25}Fe_2O_4$ added at all cooling rates. However, the maximum value of T_p varied with the ferrite content between 5 and 7 wt% for the cooling rates in the range of 5–20 °C/min. On the other hand, at 30 °C/min cooling rate, the crystallization peak increased as the ferrite content increased. The addition of this ferrite hindered the molecular transport of PEVA segments to the crystallization front and a higher super-cooling was needed for crystallization. It also limits the thickening and perfection of the PEVA crystals causing a depression in T_m and T_p. In all the cases, the crystallization enthalpy peak shifted to a lower temperature by increasing cooling rate. When the samples were cooling down at a high cooling rate, the motion of molecular chains could not follow the cooling temperature in time due to the influence of heat hysteresis, which led to a lower peak crystallization temperature. Therefore, the lower the cooling rate, the easier the crystallization.

4.4 *Non-isothermal crystallization kinetics of PEVA and $Co_{0.75}Zn_{0.25}Fe_2O_4$/PEVA system*

The integration of the exothermic peaks during the non-isothermal scans gave the relative degree of crys-

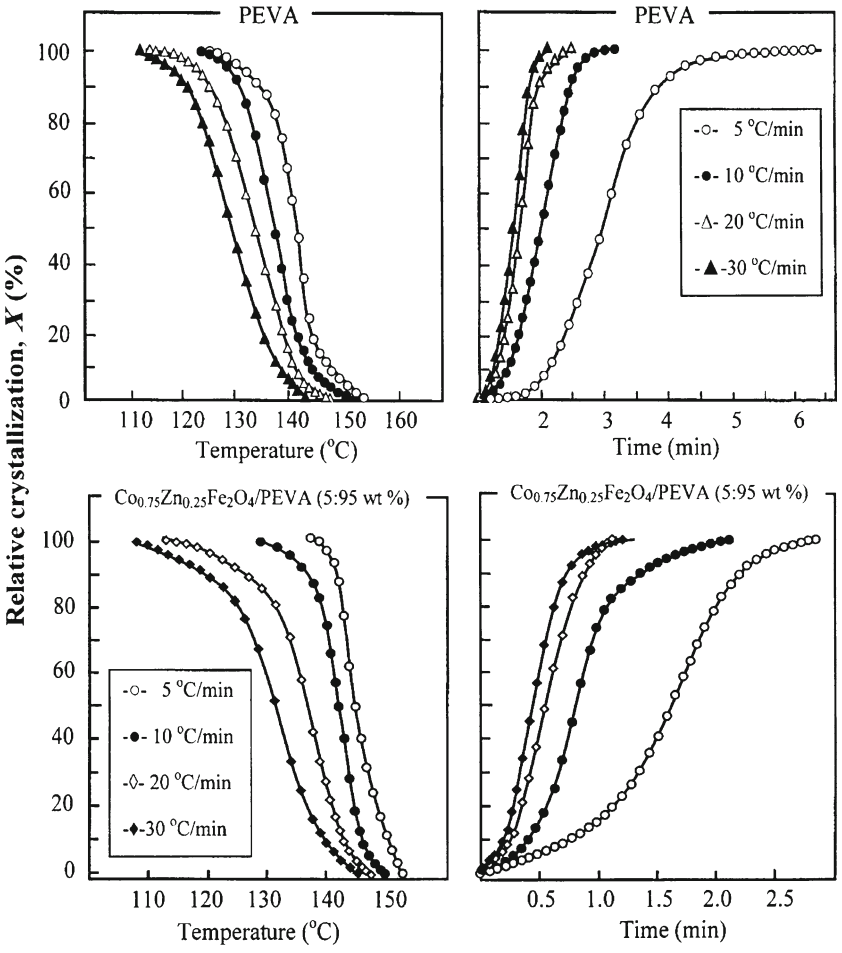

Figure 5. (**a**) Dependence of X_T on crystallization temperature and cooling rate and (**b**) dependence of X_t on crystallization time and cooling rate.

tallinity (X_T) as a function of temperature for PEVA and $Co_{0.75}Zn_{0.25}Fe_2O_4$/PEVA systems. Figure 5 shows variation of X_T vs temperature of the pure PEVA and the composite containing 5 wt% of $Co_{0.75}Zn_{0.25}Fe_2O_4$ (C_2) as a representative curve for all the composites. Because of the effect of retardation on crystallization, all curves exhibited approximately a sigmoid pattern. A typical plot of X_t vs time for PEVA and the same composite traced using the combination of (5–9) is shown in figure 5. As in the case of X_T plots vs temperature, all curves of PEVA and composites exhibited approximately a sigmoid pattern and the slopes of these curves at each point are measuring the rate of crystallization. It can be seen that the rate of crystallization was almost constant for 20–80% of the relative crystallinity because those parts of the curves were almost straight. At a later stage, the curves tended to become flat due to the spherulite impingement (Ozawa 1971).

The half time for completing crystallization ($t_{1/2}$) was estimated from the curves of figure 6 indicating the variation of X_t vs time. With an increase in $Co_{0.75}Zn_{0.25}Fe_2O_4$ content at 5 °C/min cooling rate, $t_{1/2}$ decreased dramatically and passed by a minimum value at 2 wt% of ferrite. On the other hand, at

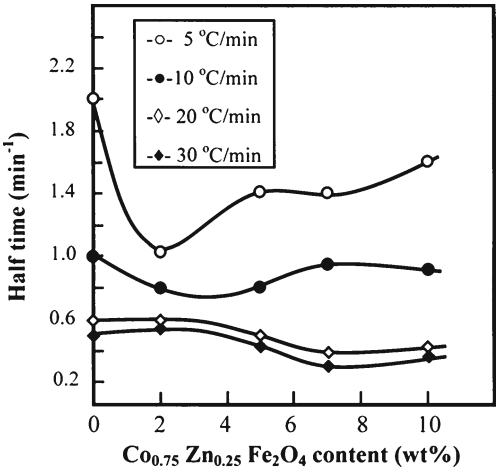

Figure 6. Variation of $t_{1/2}$ with $Co_{0.75}Zn_{0.25}Fe_2O_4$ content at various cooling rates.

10 °C/min, the minimum value of $t_{1/2}$ was observed between 3 and 4 wt% of ferrite. Below this cooling rate, no significant variation was noted. This observation can be explained by

the fact that at a relatively low $Co_{0.75}Zn_{0.25}Fe_2O_4$ content, the ferrite cluster cannot restrict the motion of the PEVA molecular chains, but act as a heterogeneous nucleating agent during the non-isothermal crystallization process and therefore, accelerates the crystallization. At a higher $Co_{0.75}Zn_{0.25}Fe_2O_4$ content, the ferrite particles cluster acts as a barrier that restricts the thermal motion of PEVA molecular chains and therefore, retards the formation of crystals. As a result, the addition of a large amount of $Co_{0.75}Zn_{0.25}Fe_2O_4$ can delay the overall crystallization process.

Plots of $\ln[-\ln(1-Xt)]$ vs $\ln(\beta)$ of PEVA and $Co_{0.75}Zn_{0.25}Fe_2O_4$/PEVA nanocomposites containing different ferrite contents showed a straight line (figure 7) indicating that the Ozawa equation (7) describes perfectly the primary process of non-isothermal crystallization of PEVA and $Co_{0.75}Zn_{0.25}Fe_2O_4$/PEVA system. The intercept and slope of $\ln[-\ln(1-X_T)]$ vs $\ln(\beta)$ yield the crystallization kinetics rate (k_T) and the Ozawa exponent (m), respectively. The

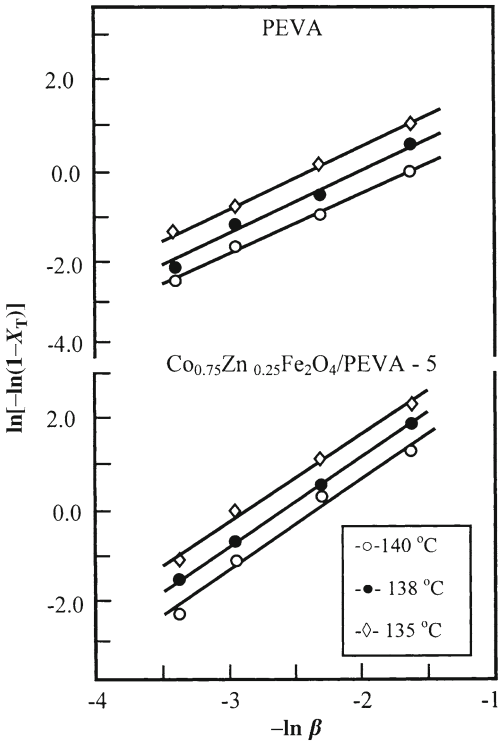

Figure 7. Ozawa plots of $\ln[-\ln(1-X_T)]$ vs $-\ln(\beta)$ for pure PEVA and $Co_{0.75}Zn_{0.25}Fe_2O_4$/PEVA system (5:95 wt%) (C_2).

results of m and k_T of PEVA and $Co_{0.75}Zn_{0.25}Fe_2O_4$/PEVA composites are gathered in table 3. It can be read from these data that the m for PEVA is practically constant in the crystallization temperature ($1{\cdot}40 \pm 0{\cdot}20$). This result is close to the literature value reported in the literature (Alvarez *et al* 2005), while the m value for $Co_{0.75}Zn_{0.25}Fe_2O_4$/PEVA systems decreased as the ferrite content and/or temperature increased. In these data it was also observed that the Ozawa exponent of the pure PEVA is lower than the composites ($1{\cdot}70$–$2{\cdot}80 \pm 0{\cdot}20$), suggesting that the introduction of $Co_{0.75}Zn_{0.25}Fe_2O_4$ content in PEVA matrix greatly influences the growth of crystals. The increase of m value from those of PEVA to those of the composites is usually attributed to the change from instantaneous to sporadic nucleation (Pratt and Hobbs 1976). According to Francis (2005), the crystallization process of PEVA is predominated by surface, while the crystallization of the ferrite/PEVA composite is predominated by bulk or three-dimensional crystal growth. The k_T value for $Co_{0.75}Zn_{0.25}Fe_2O_4$/PEVA nanocomposites was higher than those of pure PEVA. In general, it decreased significantly as the ferrite content increased. In the temperature range of 135–140 °C, it was observed that the k_T value of PEVA and all composites behaved similarly, which decreased with the increase in temperature except the one treated with 2 wt% of ferrite. For the composite prepared with 5 (C_2), 7(C_3) and 10 (C_4) wt% of $Co_{0.75}Zn_{0.25}Fe_2O_4$, the crystallization process followed the same dynamics of the pure PEVA with the variation of temperature and time. On the contrary, the one treated with 2 wt% of $Co_{0.75}Zn_{0.25}Fe_2O_4$ (C_1) is different, because at this composition the dynamic crystallization process seems to be more complex.

The crystallization activation energy (E_a) associated with the overall process of crystallization was evaluated from the rates of crystallization by using the Xu and Yinnon equation (10). Plotting $\ln\left(\beta^{n/m}/T_p^2\right) \times R/m$ vs $1/T$. E_a was obtained from the slope (figure 8). It was found that the crystallization activation energy is 233 kJ/mol for pure PEVA and increased when $Co_{0.75}Zn_{0.25}Fe_2O_4$ was added to PEVA at the limit of 7 wt% as shown in figure 9. Beyond this composition this value decreased quickly to reach 417 kJ/mol at 10 wt% of $Co_{0.75}Zn_{0.25}Fe_2O_4$ added to PEVA matrix. Similar results were observed by Peng *et al* (2005) in the study of silica/poly(vinyl alcohol) nanocomposite. These are in accord with literature reports on basis of the fact that the

Table 3. Ozawa parameter (m) and cooling function (K_T) for PEVA and $Co_{0.75}Zn_{0.25}Fe_2O_4$/PEVA nanocomposites.

	Composition of ferrite/PEVA (wt%)									
	0		2		5		7		10	
T (°C)	m	k_T	m	k_T	m	k_T	m	k_T	m	k_T
140	1·41	10·42	2·80	149·6	2·12	183·0	2·05	87·4	1·93	71·6
138	1·54	24·20	2·39	104·4	2·11	291·2	1·93	103·6	1·83	91·65
135	1·45	32·50	2·30	201·0	1·90	235·0	1·86	178·0	1·70	140·2

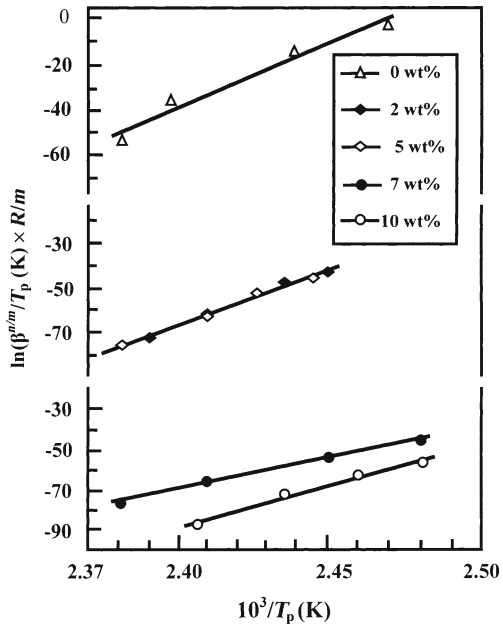

Figure 8. Plots of PEVA and $Co_{0.75}Zn_{0.25}Fe_2O_4$/PEVA (wt%) nanocomposites in accordance with Xu and Uhlmann equation.

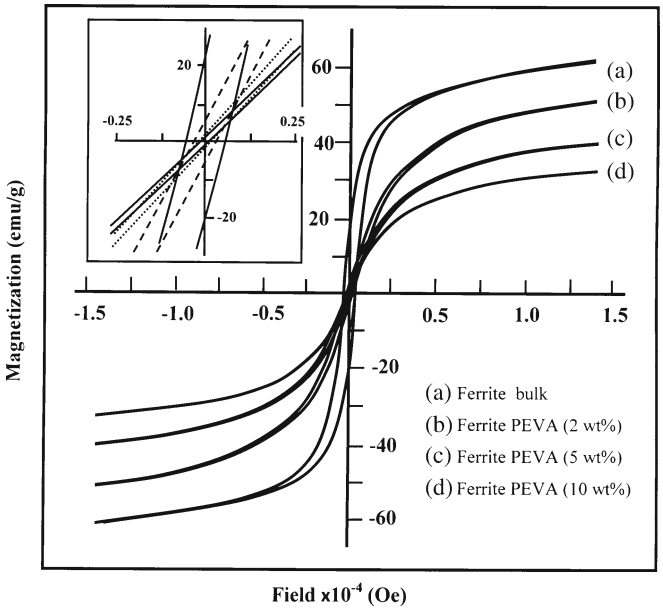

Figure 10. Magnetization vs field curves measured at 25 °C of bulk $Co_{0.75}Zn_{0.25}Fe_2O_4$ and $Co_{0.75}Zn_{0.25}Fe_2O_4$/PEVA nanocomposite at different compositions.

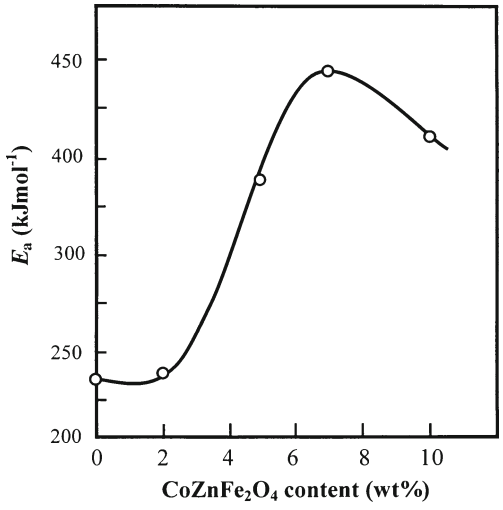

Figure 9. Variation of E_a vs composition (wt%) of $Co_{0.75}Zn_{0.25}Fe_2O_4$/PEVA system.

ferrite particles act as heterogeneous nuclei and accelerate the crystallization process at relatively low particle content. While at a higher $Co_{0.75}Zn_{0.25}Fe_2O_4$ content, these particle clusters act as a barrier to retard the crystallization by depressing the crystal growth because of the interaction between ferrite clusters and PEVA matrix.

4.5 *Magnetic properties*

Figure 10 presents profiles of magnetic hysteresis loops observed for the pure Zn-substituted cobalt ferrite ($Co_{0.75}Zn_{0.25}Fe_2O_4$) system and various $Co_{0.75}Zn_{0.25}Fe_2O_4$/PEVA composites at room temperature and applied field of 15 kOe. The different values of the saturation magnetization (M_s), remanence magnetization (M_r) and coercivity (H_c) and magnetic moment (n_B) of $Co_{0.75}Zn_{0.25}Fe_2O_4$ and various $Co_{0.75}Zn_{0.25}Fe_2O_4$/PEVA composites are summarized in table 4. Recently, our previous experiments showed that the saturation magnetization of Zn-substituted cobalt ferrite ($Co_{0.75}Zn_{0.25}Fe_2O_4$) system (58 emu/g) is greater than that of simple cobalt ferrite (45 emu/g) (Deraz and Alarifi 2012). So, in this work it has selected the previous composition of ferrite depending upon its high saturation magnetization. Inspection of figure 10 revealed that: (i) the values of M_s, M_r, M_r/M_s, H_c and n_B of different $Co_{0.75}Zn_{0.25}Fe_2O_4$/PEVA composites are smaller than that of $Co_{0.75}Zn_{0.25}Fe_2O_4$ system and (ii) for $Co_{0.75}Zn_{0.25}Fe_2O_4$/PEVA composites, the increase in the concentration of $Co_{0.75}Zn_{0.25}Fe_2O_4$ as filler led to a significant decrease in the values of M_s, M_r, M_r/M_s, H_c and n_B. The maximum decrease in the value of M_s due to the increase in the amount of ferrite (10 wt%) attained 43·31%, which corresponds to 56·9% magnetization of the filler in this composite. The treatment of PEVA with 10 wt% $Co_{0.75}Zn_{0.25}Fe_2O_4$ brought about a decrease in the values of both H_c (76·22%) and n_B (43%). The dependence of the magnetization and magnetic moment on the grain size is explained on the basis of changes in exchange interaction between tetrahedral and octahedral sublattices (Deraz and Alarifi 2012). So, we speculate that the reduction in the magnetization observed may be due to the smaller size of the $Co_{0.75}Zn_{0.25}Fe_2O_4$ particles. In fact, XRD measurements showed that the incorporation of ferrite in the polymer matrix led to decrease in the crystallite size of both ferrite and

Table 4. Magnetic parameters (M_s, M_r, M_s/M_r, H_c, n_B) of bulk $Co_{0.75}Zn_{0.25}Fe_2O_4$ and $Co_{0.75}Zn_{0.25}Fe_2O_4$/PEVA nanocomposites determined at room temperature.

System ferrite/PEVA (g:g)	M_s (emu g^{-1})	M_r (emu g^{-1})	M_s/M_r	H_c (Oe)	n_B
100:0	58	23·12	2·51	536·5	2·53
2:98	52	6·23	8·35	313·0	2·20
5:95	40	2·62	15·27	156·1	1·69
10:90	33	1·23	26·83	127·6	1·40

polymer. In addition, the lower value of M_s of the composite is probably due to larger part in the incorporation of ferrite nanoparticles into the polymer matrix which added mass of the thick polymer layer on the ferrite nanoparticles (Chertok *et al* 2008). Similar study on synthesis, characterization and magnetic properties of ferrite–polymer nano-composite spheres prepared from $NiFe_2O_4$ or $Ni_{0.5}Zn_{0.5}Fe_2O_4$ and hydrophilic polymers such as polyhydroxylated methylmethacrylate (PHPMMA) or polyvinyl alcohol (PVA) is reported (Sindhu *et al* 2006).

5. Conclusions

SEM images revealed that the magnetic particles as filler are nanosize, randomly oriented, uniformly dispersed and isolated from each other. Ruling out the tendency to form agglomerates in the ferrite–polymer samples even at a relatively high loading level. However, incorporation of the ferrite powders in the polymer matrix may lead to a modification in the different properties of the polymer studied as well as formation of a new polymer-bonded magnet. XRD patterns indicated that the incorporation of the ferrite powder in the polymer matrix led to a decrease in the degree of crystallinity of the polymer reflected by the decrease in the peak height of the polymer.

From the DSC results it was concluded that the Ozawa equation describes perfectly the primary process of non-isothermal crystallization of PEVA and $Co_{0.75}Zn_{0.25}Fe_2O_4$/PEVA systems. Through this model, it was confirmed that the $Co_{0.75}Zn_{0.25}Fe_2O_4$ was distributed uniformly throughout PEVA matrix. The introduction of $Co_{0.75}Zn_{0.25}Fe_2O_4$ content in PEVA matrix greatly influence the growth of crystals and the crystallization process of PEVA has been predominated by surface, while the crystallization of the ferrite/PEVA composite is predominated by bulk or three-dimensional crystal growth. The crystallization process followed the same dynamic of the pure PEVA with variation in temperature and time. On the contrary, one treated with 2 wt% of $Co_{0.75}Zn_{0.25}Fe_2O_4$ was different, at this composition the dynamic crystallization process seemed to be more complex.

In general, it was found that the crystallization activation energy (E_a) increased when $Co_{0.75}Zn_{0.25}Fe_2O_4$ was added to PEVA at the limit of 7 wt%. Beyond this composition, this value decreased quickly. The ferrite nanoparticles were uniformly distributed throughout the PEVA matrix and at the room temperature. VSM measurements indicated that magnetica particles incorporated in PEVA were superparamagnetic. The $Co_{0.75}Zn_{0.25}Fe_2O_4$/PEVA systems are promising magnetic drug carriers to be used in magnetically targeted drug delivery.

Acknowledgements

The authors thank the Research Centre of Faculty of Science – King Saud University for the financial support.

References

Alvarez V A, Stephani P M and Vazquez A 2005 *J. Therm. Anal. Cal.* **79** 187
Arshady R 1993 *Biomaterials* **14** 5
Avrami M J 1937 *J. Chem. Phys.* **7** 1103
Boolchand P 2006 *J. Appl. Phys.* **99** 08G702
Chertok B, Moffat B A, David A E, Yu F Q, Bergemann C, Ross B D and Yang V C 2008 *Biomaterials* **29** 487
Cullity B D 1976 *Elements of X-ray diffraction* (Addison-Wesly Publishing Co. Inc.) (Chapter 14)
Deraz N M and Alarifi A 2012 *J. Anal. Appl. Pyrolysis* **94** 41
Deraz N M, El-Aiashy M K and Ali S A 2009 *Ads. Sci. Tech.* **27** 797
Francis A A 2005 *J. Am. Ceram. Soc.* **88** 1859
Gomez-Lopera S A, Plaza R C and Delgado A V 2001 *J. Coll. Interf. Sci.* **240** 40
Guschl P C, Kim H S and Otaigbe J U 2002 *Appl. Polym. Sci.* **83** 1091
Hammami A, Pruiell J E and Mohrotra A K 1995 *Polym. Eng. Sci.* **35** 797
Jeziorny A 1978 *Polymer* **19** 1142
Kazantseva N E, Bespyatykh Y I, Sapurina I, Stejskal J, Vilcakova J and Saha P 2006 *J. Magn. Magn. Mater.* **301** 155
Keskin S and Elliot J R 2003 *Ind. Eng. Chem. Res.* **42** 6331
Kissinger H E 1956 *J. Res. Natl. Bur. Stand. (US)* **57** 217
Kuo S W, Liu W P and Chang F C 2005 *Macromol. Chem. Phys.* **206** 2307
Li C, Kong Q, Fan Q and Xia Y 2005 *Mater. Lett.* **59** 773
Lin J H, Moo E M and Hung Y P 2006 *J. Polym. Sci. B: Polym. Phys.* **44** 3357
Matsumoto M and Miyata Y 2002 *J. Appl. Phys.* **91** 9635
Montoya M, Abad M J, Bara L and Bernal C 2006 *Eur. Polym. J.* **42** 263
Nakamura T, Tsutaoka T and Hatakeyama K 1994 *J. Magn. Magn. Mater.* **138** 319

Ozawa T 1971 *Polymer* **12** 150
Pant R P, Rashmi R, Krishna M, Negi P S, Ravat K, Dhawan U, Gupta S K and Suri D K 1995 *J. Magn. Magn. Mater.* **149** 10
Peng Z, Kong L X and Li S D 2005 *Polymer* **46** 1949
Pratt C F and Hobbs S Y 1976 *Polymer* **17** 12
Sindhu S, Jegadesan S, Parthiban A and Valiyaveettil S 2006 *J. Magn. Magn. Mater.* **296** 104
Slama J, Gruskova A, Vicen R, Vicenova S, Dosoudil R and Franek J 2003 *J. Magn. Magn. Mater.* **642** 254
Utracki L A, Favis B D and Nicholas P 1989 *Composites and specialty applications* (ed.) Cheremisinoff, *Handbook of Polym. Sci. and Tech.* vol. 4 (New York: Marcel Dekker Inc.)
Vaishnava P P, Senaratne U, Buc E, Naik R, Naik V M, Tsoi G M, Wenger L E and Boolchand P 2006 *J. Appl. Phys.* **99** 08G702
Wiltshire M C K, Pendry J B, Young I R, Larkman D J, Gilderdale D J and Hajnal J V 2001 *Science* **291** 849
Xiao J and Otaigbe J U 2000 *Polym. Compos.* **21** 332
Xu X J, Ray C S and Day D E 1991 *J. Am. Ceram. Soc.* **74** 909
Yavuz O, Ram M K, Aldissi M, Poddar P and Hariharan S 2005 *J. Mater. Chem.* **15** 810
Yinnon H and Uhlman D R 1983 *J. Non-Cryst. Sol.* **54** 253
Young T H, Lai J Y, You W M and Cheng L P 1997 *J. Membr. Sci.* **128** 55
Ziabicki A 1996 *Coll. Polym. Sci.* **274** 209